International Journal of Materials Engineering and Technology
Volume 6, Number 1, 2011, Pages 11-26
Published Online: September 2011
This paper is available online at http://pphmj.com/journals/ijmet.htm

TRANSFORMATION DIAGRAM DETERMINATION USING IMPACT TESTING

B. W. KING and L. S. CHUMBLEY

Iowa State University
214 Wilhelm Hall
Ames, IA 50011-3020, U.S.A.

Abstract

Superaustenitic alloys are chosen for their combination of high strength, toughness, and corrosion resistance. The motivation for this study was to develop a time-temperature transformation (TTT) diagram for the superaustenitic stainless steel CN3MN at short heat treatment times. This was done through the use of Charpy impact tests and an experimental matrix of times, 0 sec to 960 sec, and temperature, 593°C to 982°C. Impact strength loss as a function of both time and temperature was determined. In proper heat treatments the superaustenitic stainless steel CN3MN has extremely high impact strength, therefore, to ensure the samples would break on a standard 300 ft-lb machine half-size samples were tested. The resulting fracture surfaces were examined using optical and scanning electron microscopy (OM, SEM) and energy dispersive spectroscopy (EDS). Qualitatively differences in compositions between the bulk and brittle fracture surfaces were measured. Samples heat-treated at or above 843°C display a significant drop in impact strength within 960 sec. SEM analysis of fracture surfaces exhibit a transition from ductile to brittle fracture as impact strength decreases. The TTT diagram for these short times as well as analysis of the fracture surfaces will be discussed.

1. Introduction

Duplex and superaustenitic stainless steels are engineered to provide superb

Keywords and phrases: impact testing, CN3MN, superaustenitic, embrittlement.

Received May 18, 2011

crevice and pitting corrosion resistance during both seawater and high temperature applications. Corrosion resistance is achieved by the heavy alloying of Cr, Ni, and Mo in Fe. Minor additions of Cu, Mn, N, Si, and W may also be present in some specific alloys further reducing the overall amount of Fe in superaustenitic stainless steels to below 50%. While heavy alloying enhances corrosion performance it also promotes the formation of carbides, nitrides, and intermetallic compounds. The formation of these various compounds occurs rapidly upon heat treatment if not done correctly [2, 8, 9]. Examination of the microstructure of several highly alloyed steels as a function of heat treatment has shown intermetallics are the first phases to form [3, 6, 7, 13, 15]. Sigma (σ), chi (χ), and laves phases have been observed in studies involving long term phase transformations [6, 7, 10, 13], with initial nucleation favoring high-Mo content intermetallic formation along grain boundaries [2]. The complete transformation of superaustenitic stainless steels from solid solution to the thermodynamic equilibrium assemblage of phases is very sluggish and does not occur for up to three months at elevated temperatures [7].

Ensuring superaustenitic stainless steels maintain their optimum strength and corrosion resistance during processing and service life is essential. Previous phase transformation studies have shown that precipitate phases are slow to obtain significant volume fractions [6]. For example, the Duplex and superaustenitic stainless steels show a significant growth of precipitates (> 5 vol%) only after extended exposure to elevated temperatures [5, 8, 13]. Several studies have suggested that mechanical properties such as tensile strength and hardness are not adversely affected until at least 5 vol% of precipitates is present in the matrix [5, 8, 13]. Despite these results, improper heat-treatments have been shown to cause a reduction in impact strength in extremely short time periods. Several studies have suggested intermetallic phase formation is the cause [1, 2, 9], although examination of the microstructure [2] reveals that minuscule amounts (< 1 vol%) of precipitation can be detected, far below the 5 vol% level.

One possible reason for the rapid embrittlement seen in highly alloyed steels is an inadequate initial solution heat treatment. Studies by Dupont [4] have shown that extended times at high temperatures are necessary to dissolve unwanted phases in the bulk material. In some cases where the amount of Mo additions are high, which is common for many superaustenitic stainless steels, studies have found that currently specified heat treatments may fail to adequately distribute the Mo [4, 11, 12].

The specific objective of this research was to determine the loss of impact strength as a function of both time and temperature in the alloy CN3MN. Impact strength has been shown to be a very sensitive means by which embrittlement and precipitation formation can be detected [1]. Observation of the resultant data was used to construct a time-temperature transformation (TTT) diagram for CN3MN that is applicable at extremely short time heat treatments.

Experimental Procedure

For this study material was solicited from a number of foundries associated with the Steel Founders Society of America (SFSA). The alloy CN3MN was received in the as cast condition in the form of keel bars and the letters A through F were used to label the six foundries that contributed material. Keel bars ranged in size from $1'' \times 8''$ round cylinders to $1.5'' \times 1.5'' \times 7''$ bars. Chemical specifications for the bars all stated that the heats were all within ASTM specifications. As an independent check of this a small section of a keel bar from each received heat was sent for chemical analysis using optical emission spectroscopy (OES), and the range of experimental compositions found is shown in Table I. Note that some of these values fall slightly outside the specified range for CN3MN.

All of the keel bars were solution heat-treatment at 1204°C for 4 hours immediately followed by a water quench. After solution heat-treatment the bars were machined to ASTM E-23 standard half size Charpy blanks, $5\text{mm} \times 10\text{mm} \times 55\text{mm}$ in size, both by cooperating SFSA foundries and by resources available in Ames Laboratory (AL) on the Iowa State University (ISU) campus. Half size specimens were chosen to ensure that all of the specimens would fracture at room temperature using a standard 300 ft-lb Charpy Impact Tester. The Charpy blanks were then uniformly notched using electrical discharge machining (EDM) by AL. Completed Charpy specimens were encapsulated in a quartz tube under an inert argon atmosphere in sets of 3. Heat treatments were performed using a vertical tube furnace. Specimens were elevated directly into this furnace, which was already operating at the desired set temperature. Temperature was monitored by means of a control sample, especially machined for this purpose, that consisted of a full size, $10\text{mm} \times 10\text{mm} \times 55\text{mm}$, Charpy specimen with a thermocouple inserted in the center of the specimen, Figure 1. The control specimen was secured to the quartz encapsulation tube containing three specimens. Both tube and control were then raised into the hot zone of the furnace at the same time. The clock for counting the

duration of the heat treatment was started when the temperature of the control specimen was within 5°C of the desired set temperature. On average the desired set temperature was reached within 400 seconds of insertion. After the specified time had elapsed the tube was quickly lowered and the specimens were water quenched, with the quartz tube being broken when under water to speed the quench.

Table I. Average composition for keel blocks used in this study.

Element	Foundry A	Foundry B	Foundry C	Foundry D	Foundry E	Foundry F	CN3MN (nominal)
C	0.017	0.016	0.024	0.014	0.029	0.023	< 0.03
Mn	0.51	0.88	1.12	0.98	0.8	1.44	< 2.0
Si	0.6725	0.75	0.63	0.76	0.78	0.37	< 1.0
S	0.007	0.004	0.004	0.008	0.009	0.009	< 0.01
P	0.01875	0.011	0.016	0.017	0.023	0.017	< 0.04
Cr	20.775	21.69	21.1	19.65	20.98	20.8	20.0 to 22.0
Ni	24.665	24.12	24.8	25.82	26.04	25.44	23.5 to 25.5
Mo	6.375	6.54	6	6.46	5.36	6.22	6.0 to 7.0
N	0.181	0.204	0.185	0.168	0.235	0.191	0.18 to 0.26
Cu	0.1	0.03	0.24	0.11	0.21	0.35	< 0.75

Figure 1. Sample holder with control specimen. White arrow indicates thermocouple position in the center of the control specimen.

Heat treatments were carried out at the temperatures specified in Table II for material received from Foundries A-E. (N.B. Material from Foundry F was received much later and is discussed later as a separate study). Different times were tested at each heat treatment temperature, from a minimum of 0 seconds (i.e., at the moment the sample was 5˚C below the desired temperature) up to 960 seconds. Impact strength testing at room temperature was accomplished using a calibrated and instrumented 400 ft-lb Tinius Olsen Charpy impact tester located at the Caterpillar Technical Center in Peoria, Illinois. Six specimens in the as-solution-heat-treated condition were tested for a baseline.

Table II. Temperature and Time Matrix

Temp(˚C)	982	927	899	871	843	816	760	704	648	593
Time (sec)	0	30	60	120	240	480	960			

Further examination of the microstructure was performed using optical and scanning electron microscopy (OM, SEM). Specimens were prepared for analysis from the fractured Charpy samples using standard metallographic techniques. The samples' fracture surfaces were characterized using a JEOL 6060LV scanning electron microscope (SEM) and energy dispersive spectroscopy (EDS) was employed to obtain qualitative compositional analysis from the fracture surfaces.

Experimental Results

Fracture toughness

The as-solution-heat treated strengths of the six specimens ranged from a low of 86.3 J to a maximum of 152.3 J, with the average being 106.0 J. Impact strength data for the room temperature Charpy tests for each temperature is plotted in Figure 2. As a first approximation the data was described using a linear fit at each temperature. This is believed to be a reasonable assumption since a classic Avrami plot of percent transformation can be approximated as a linear decrease in the initial stages. The equation for the best fit line and R^2 value are displayed on each graph.

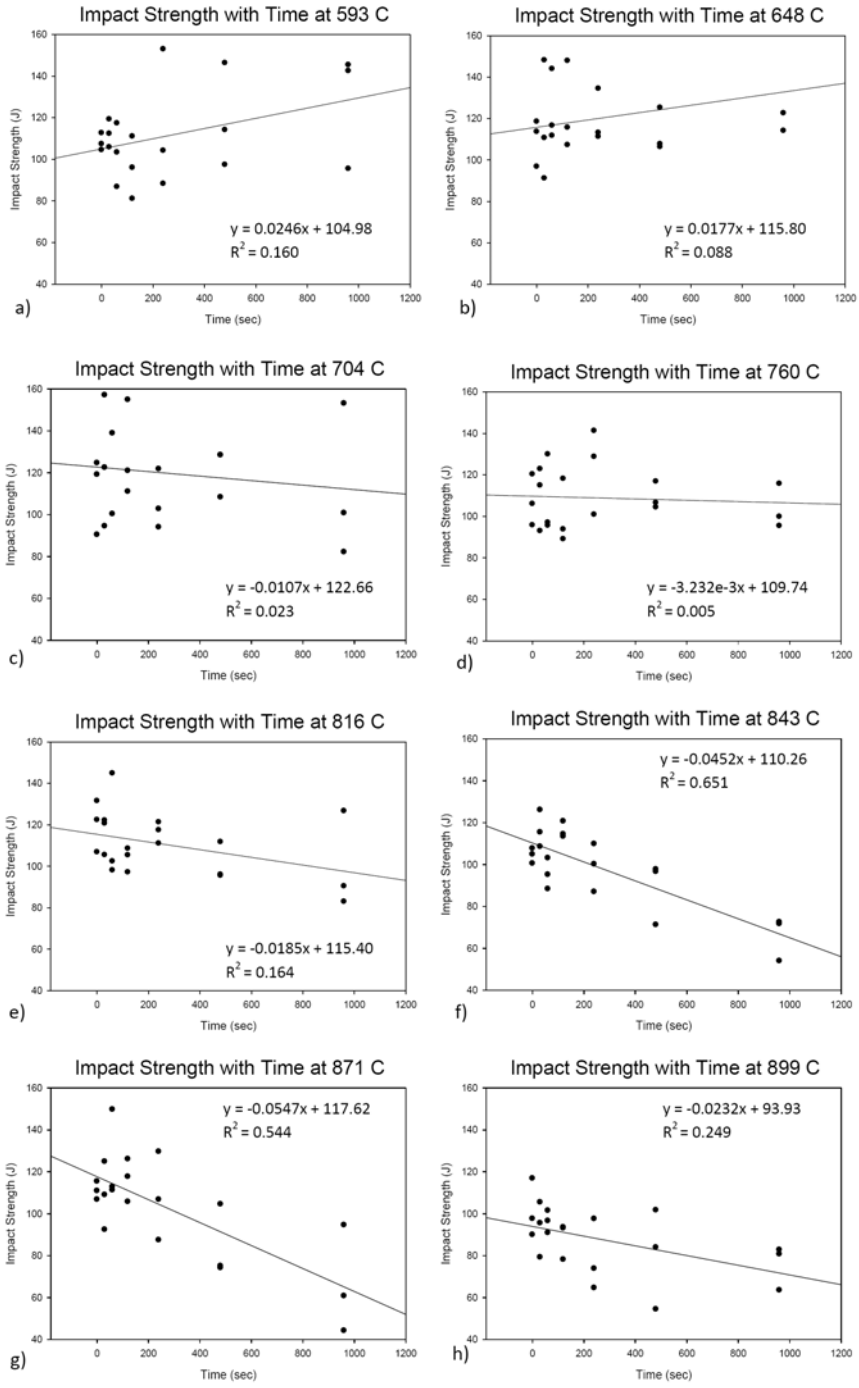
Impact Strength with Time at 593 C
y = 0.0246x + 104.98
R2 = 0.160
a)
Impact Strength with Time at 648 C
y = 0.0177x + 115.80
R2 = 0.088
b)
Impact Strength with Time at 704 C
y = -0.0107x + 122.66
R2 = 0.023
c)
Impact Strength with Time at 760 C
y = -3.232e-3x + 109.74
R2 = 0.005
d)
Impact Strength with Time at 816 C
y = -0.0185x + 115.40
R2 = 0.164
e)
Impact Strength with Time at 843 C
y = -0.0452x + 110.26
R2 = 0.651
f)
Impact Strength with Time at 871 C
y = -0.0547x + 117.62
R2 = 0.544
g)
Impact Strength with Time at 899 C
y = -0.0232x + 93.93
R2 = 0.249
h)
Impact Strength (J)
Time (sec)

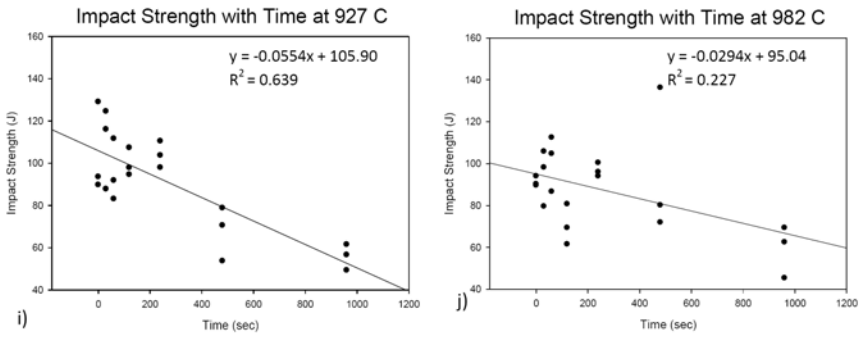

Figure 2. Impact Strength with respect to heat treatment time at (a) 593°C, (b) 648°C, (c) 704°C, (d) 760°C, (e) 816°C, (f) 843°C, (g) 871°C, (h) 899°C, (i) 927°C, and (j) 982°C.

At temperatures below 815°C the impact strength shows little or no drop in toughness, with a slight toughening possibly occurring at the lowest temperatures. Starting at 815°C the impact strength shows a steady decrease at temperatures up to the maximum tested of 982°C.

Scanning electron microscopy

Analysis of the fracture surfaces confirms a change in failure mode in the temperature range 815˚C to 843˚C from ductile to brittle fracture as a function of time, while samples heated below 815°C show little or no drop in fracture toughness. For example, the SEM images of a fracture surface of a sample heat treated at 593˚C for 0 seconds are shown in Figure 3. The fracture surface displays characteristic dimpling of the surface indicative of microvoid coalesence.

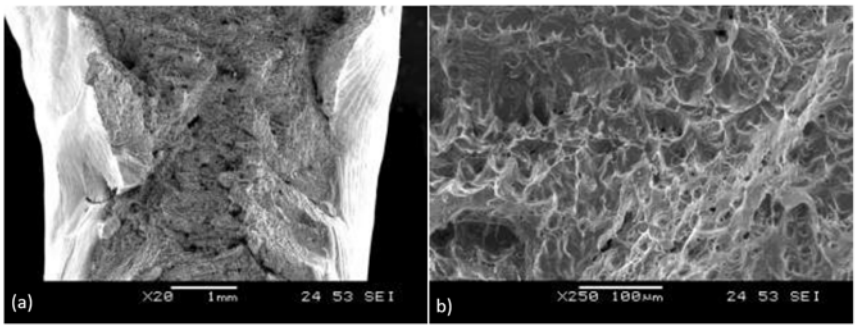

Figure 3. SEM image of high impact strength fracture (a) at 20x magnification and (b) at 250x magnification.

An example of brittle fracture is shown in Figure 4. This specimen was heat treated at 968˚C for 960 seconds and contains large areas of intergranular brittle fracture. This particular sample showed a drop in impact strength of over 50%.

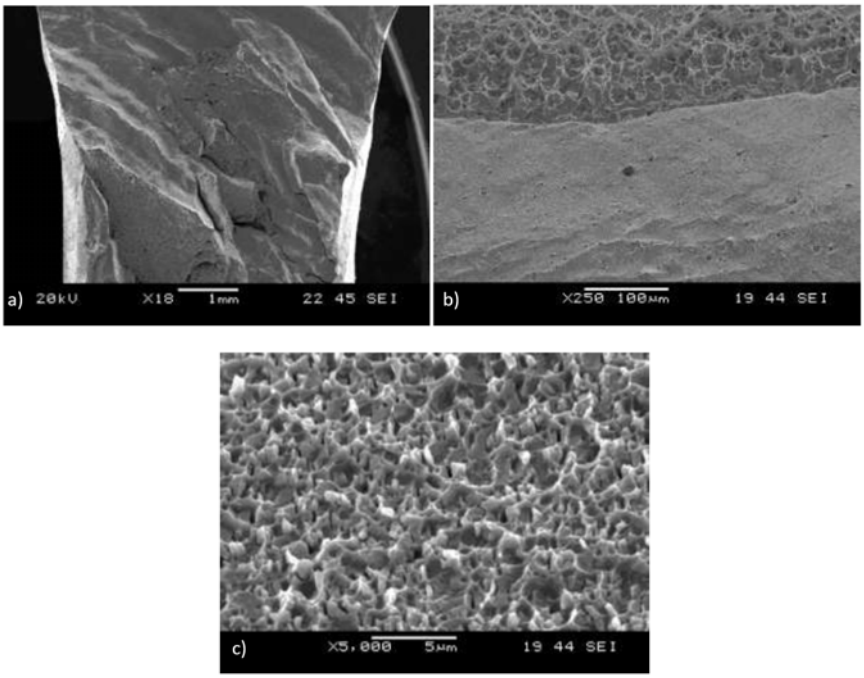

Figure 4. SEM images of low impact strength fracture surface at (a) 20x. Transitional fracture surface (b) at 250x. (c) 5000x magnification of the brittle fracture surface.

Chemical analysis using EDS was carried out on both bulk and brittle appearing areas, and the results are shown in Table III. The nominal analysis was conducted on polished samples and represents an average of seven sampled regions. Seven regions from brittle surfaces were also sampled, the points considered being chosen to be as flat as possible to approximate as closely as possible the ideal of having a polished sample for quantitative analysis. Although the nature of the analysis (i.e., unpolished sample) limits the reliability of the quantitative numbers obtained from the brittle regions, it is clear that qualitatively the brittle surfaces contain a much higher percentage of Mo and Si than the bulk.

Table III. Qualitative analysis of weight percent composition of material and brittle fracture surfaces

Element	Nominal	Brittle Surface
Si	1.61	2.95
Cr	21.94	22.67
Mn	0.89	0.92
Fe	48.29	45.58
Co	0.26	0.29
Ni	24.06	23.43
Cu	0.34	0.32
Mo	2.62	3.84

Discussion

A transformation diagram for CN3MN was constructed using the linear best fit trend lines shown in Figure 2. It should be noted that even samples listed at 0 seconds still have been subjected to thermal effects during the heating cycle since 0 represents the time taken to raise the sample to the desired set temperature followed by an immediate quench. Thus, the averaged value for material in the as-solution treated condition, i.e., 106.3 J, was used as the value for initial impact strength of the specimens before undergoing heat treatment. Observation of the data shows a large number of samples, particularly at the lower temperature heat treatments, have a higher value than this overall average. It is uncertain whether this indicates that a slight strengthening has occurred at the lower temperatures or whether this is just a result of scatter in the data. In either event, the averaged as-solution-heat-treated value was used for all subsequent calculations of percentage strength loss to maintain consistency when comparing the data.

Since the average fracture toughness of the solution heat treatment strength was 106.3 J, a loss of 10.6 J was assumed to be associated with a 10% loss in impact strength. The best fit line for each specific heat treatment was then examined and the point at which a drop of 10% from the solution heat treated was noted. The time associated with this loss, which is assumed to represent an average 10% over-all loss

in solution heat treated strength, was then plotted on the transformation diagram. A sample calculation for a 10% loss at 843˚C is shown below.

$$10\%\ \text{Loss in Strength} = 106.3J - (106.3 \times 0.1)J = 95.67J$$

Setting the Best Fit line for 843˚C equal to a 10% Loss in Strength

$$x = \text{time in seconds}$$

$$95.67J = -0.0452x + 110.26$$

$$X = 323\ \text{seconds}$$

At 843˚C a sample will have lost 10% of its solution heat treated strength in 323 seconds.

Following the example calculation above and solving for 10%, 20%, and 30% loss in impact strength for all temperatures, a transformation diagram can be obtained. This is done in Figure 5, which shows a transformation curve for embrittlement of CN3MN for the range 704˚C to 982˚C. Values for 593˚C and 649˚C were omitted due to the fact that they showed no noticeable loss in strength and, in fact, showed a slight increase in toughness. The rapid rate of embrittlement of CN3MN at temperatures above 843°C is highlighted in an enlarged section of the TTT curve shown in Figure 6.

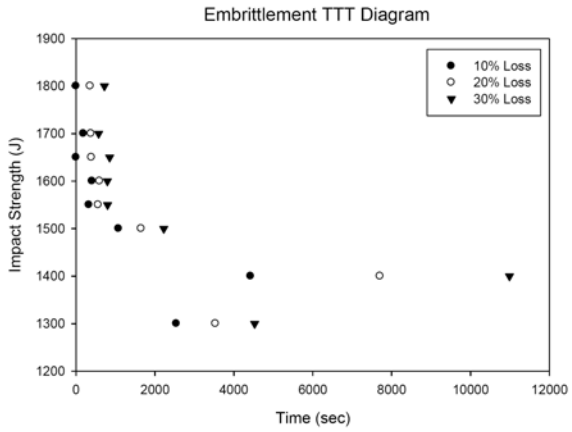

Figure 5. Impact strength loss at 704°C to 982°C.

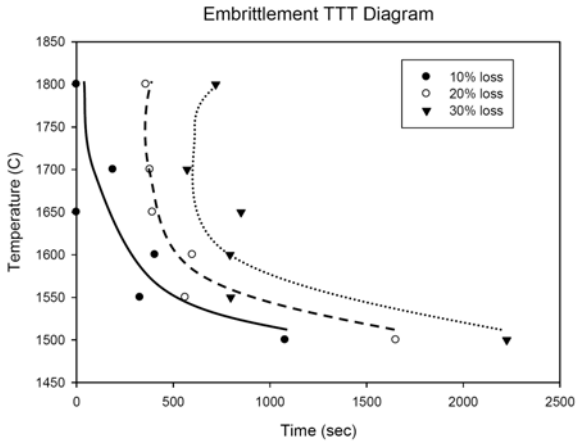

Figure 6. Impact strength loss at 816°C to 982°C.

Examination of the transformation diagram shows that at both 899°C and 982°C the samples have undergone a 10% percent loss in strength by the time they reach the set temperature, due simply to the heating that occurs during the time required to reach temperature. This would imply that during that time the specimen was undergoing a transformation very rapidly.

There is a considerable amount of scatter in the data. This is accounted for by the fact that material from different foundries and different heats was used for this study. Although the heat compositions received with the keel bars all met specifications, as was noted above independent chemical analysis of the actual keel bars showed that the composition varied substantially. For example, one particular set of keel bars from Foundry E was found to be low in Mo content by about 1 wt%. Examination of the data obtained from the Charpy specimens machined from these keel bars found that they consistently showed lower initial fracture toughness. However, this was compensated for by a slower embrittlement rate, i.e., these samples held their strength as a function of time at temperature much better than did the remaining samples which were quite uniform in composition. These results would tend to support the earlier studies that have shown high Mo phases to be the first intermetallics to form [2, 4].

Although not specifically studied by this project, it is clear that composition plays an important role in the kinetics of embrittlement. As this study was designed to represent conditions that exist within the industry, samples were taken from various heats provided by cooperating companies with no effort made to ensure that

all samples contained exactly the same composition. However, earlier studies on duplex alloys have shown that small changes in composition can lead to dramatic effects in precipitation, and which intermetallic phase is the initial precipitate [13, 15].

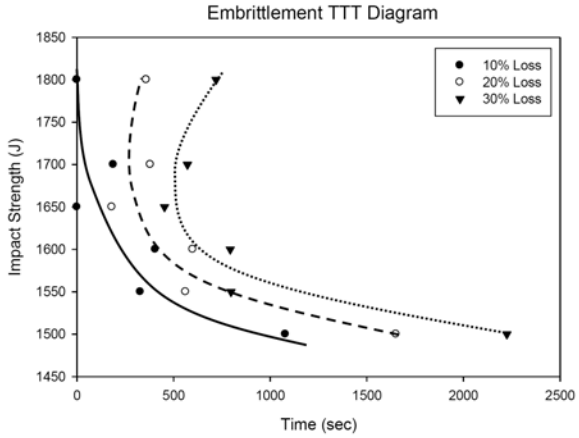

Figure 7. Embrittlement TTT diagram with Foundry E removed from the calculation.

One effect of composition on the TTT curve determined in this study can be seen if the data from Foundry E is deleted from the analysis, where the amount of Mo in the keel bar (if not the overall heat as given by the provided analysis) was determined to be low. This is shown in Figure 7. Note that the nose shifts from around 927°C to 899°C, and that the data holds a more consistent trend. This would indicate that Mo particularly is likely to promote early precipitation from solution. This is in agreement with previous work that has shown that initial precipitation in highly alloyed steels is usually the Laves phase or the Chi phase, both of which are higher in Mo than the sigma phase [8-10]. It also is in agreement with studies concerning the diffusion rates of Mo in highly alloyed steels and that extended times and high temperatures must be used in order to obtain a homogenous structure [4, 11, 12].

Given the importance of composition noted above a further study was undertaken using material from a single foundry, designated F, to study variation within a single source of material. The composition of the received material is shown in Table I. This material was given the same solution heat treatment as for material from Foundries A-E and samples were then subjected to temperatures of 816°C,

885°C, and 913°C for times in the range 500 to 3000 sec at 816°C and 250 to 1000 sec for 885°C and 913°C. These temperatures and times were chose as an attempt to refine the nose of the TTT curve shown in Figure 7. The results from this small study are shown in Figure 8.

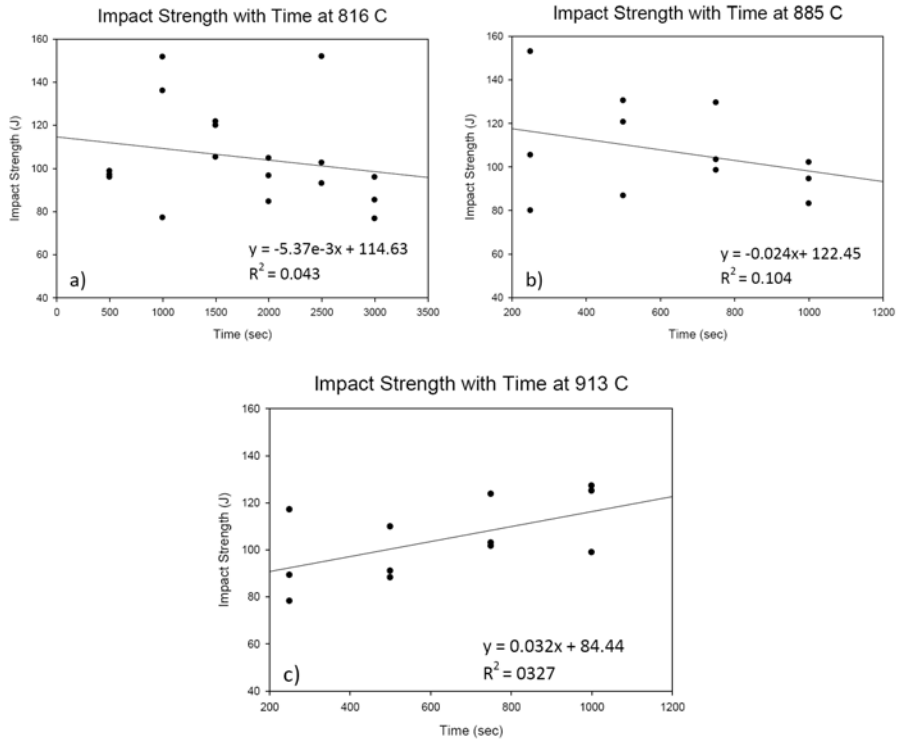

Figure 8. Impact strength with respect to heat treatment time at (a) 816°C, (b) 885°C, and (c) 913°C.

The data at 816°C and 885°C follow a similar pattern to the initial study, i.e., a decreasing impact strength with respect to time. However, samples tested at 913°C surprisingly show a slight increase in strength with time. It is important to note that the material from Foundry F had the lowest intercept of any of the data at 84.44 J. All of the other data (Figure 2) show an extrapolated intercept in the range 93-122 J. Thus, the data at 913 °C is anomalous and produces negative values in the calculations used, producing nonsensical values if one attempts to incorporate the data into the diagram of Figure 7. For this reason none of the data from Foundry F was included in Figure 7.

It has already been noted that the low Mo composition of material from Foundry E can be seen to change the TTT curve substantially. The composition of material from Foundry F is noted to be slightly higher in Cu and Mn, but it is unknown whether this is the cause for the observed anomaly in impact strength. While Figure 7 gives a good initial diagram covering a broad range of foundries, heats, and compositions, a matrix of samples where the composition is controlled more stringently than specified in current standards is necessary if one wishes to develop a more rigorous diagram.

It is clear from this study that while TTT diagrams can be developed fairly easily using impact strength large variability in the data exists and must be taken into account. If a question arises as to whether any particular heat might be susceptible to embrittlement it may be wise to conduct impact tests on samples machined from heat keel bars and examine the fracture surface for regions of brittle failure. Clearly, further study is required to completely elucidate the dramatic effect of composition on the impact properties of this specific alloy.

Summary and Conclusions

The superaustenitic stainless steel CN3MN undergoes a rapid loss in impact strength when heat treated in the range 843°C to 982°C. The loss can be as great as 30% percent of the as-solution heat treated value for times as short as 960 seconds, with a 10% loss being seen almost immediately upon heating to these temperatures. The nose of the TTT curve begins near 899°C. Fracture surfaces of CN3MN with low impact strength display high levels of brittle fracture and surface compositions high in Mo, indicating that formation of a Mo-rich precipitate on grain boundaries is the most likely reason for the embrittlement. This is supported by previous studies in the duplex alloys and by the observation that data keel bars that were found to be somewhat low in Mo had lower initial strengths but were more resistant to embrittlement than those with higher Mo additions.

Acknowledgments

The authors would like to acknowledge the Steel Founders Society of America and their member companies for their considerable assistance in this project, without whose help this research would not have been possible. We especially would like to acknowledge Metaltek, Spuncast, Stainless Foundry, Bradken Atlas, American

Foundry, Monnet Metals, and Howell Foundry for providing machining assistance, samples for study, and chemical analysis. The authors are also thanks for the assistance and support of Caterpillar, Inc. of Peoria, Illinois and Mr. Pete Dawson for his support and use of their Charpy impact equipment. A portion of this work was carried out using facilities of the Ames Laboratory. Ames Laboratory is operated for the U.S. Department of Energy by Iowa State University under Contract No. DE-AC02-07CH11358.

References

[1] C. D. Lundin and V. Hariharan, Behavior of Duplex Stainless Steel Castings, Volumes 1-5, U.S. Department of Energy, 2005.

[2] C. Muller and L. S. Chumbley, Fracture toughness of heat treated superaustenitic stainless steels, Journal of Materials Engineering and Performance (2009), 714-720.

[3] E. Johsnon, Y. Kim, L. S. Chumbley and B. Gleeson, Preliminary phase transformation diagram determination for the CD3MN cast duplex stainless steel, Scripta Materialia (2004), 1351-1354.

[4] J. D. Farren and J. N. Dupont, Heat treatment of high alloy stainless steel castings, Technical and Operating Conference, Steel Founders Society of America, Chicago, IL, 2006.

[5] M. Blair, Special Report Number 31, Steel Founders Society of America, Crystal Lake, IL, 2001, pp. 1-52.

[6] N. Phillips, L. S. Chumbley, B. Gleeson and O. Ugurlu, Determination of phase transformations in cast superaustenitic stainless steels, Technical and Operating Conference, Steel Founders Society of America, Chicago, IL, 2006.

[7] N. S. L. Phillips, L. S. Chumbley and B. Gleeson, Phase transformation in cast superaustenitic stainless steels, Journal of Materials Engineering and Performance (2009), 1285-1293.

[8] S. Heino, M. Knutson-Wedel and B. Karlsson, Precipitation in a high nitrogen superaustenitic stainless steel, Material Science Forum (1999), 143-148.

[9] S. Heino, Role of Mo and W during the snesitization of superaustenitic stainless steel-crysallography and composition of precipitates, Metallurgical and Materials Transformation (2000), 1893-1905.

[10] S. Milan, A. Kroupa, J. Sopousek, J. Vrestal and P. Miodownik, Phase changes in superautenitic steels after long-term annealing, Z. Metallkd. (2004), 1025-1030.

[11] S. W. Banovic, J. N. DuPont and A. R. Marder, Dilution and microsegregation in dissimilar metal welds between super austenitic stainless steel and nickel based alloys, Science and Technology of Welding and Joining (2002), 374-383.

[12] T. D. Anderson, J. N. Dupont, A. R. Marder and M. J. Perricone, The influence of molybdenum on stainless steel weld microstructures, Welding Journal (2007), 281-292.

[13] Y.-J. Kim, L. S. Chumbley and B. Gleeson, Continuous cooling transformation in cast duplex stainless steels CD3MN and CD3MWCuN, Journal of Materials Engineering and Performance (2008), 234-239.

[14] Y.-J. Kim, L. S. Chumbley and B. Gleeson, Determination of isothermal transformation diagrams for sigma-phase formation in cast duplex stainless steels, Metallurgical and Materials Transactions (2004), 3377-3386.

[15] Y.-J. Kim, O. Ugurlu, C. Jiang, B. Gleeson and L. S. Chumbley, Microstructural evolution of secondary phases in the cast duplex stainless steels CD3MN and CD3MWCuN, Metallurgical and Materials Transactions (2007), 203-211.